



# Fabrication and Performance of Multi-wall Carbon Nanotubes Reinforced Polyimide Electrospun Nanofiber Membranes

Shenbing Cao<sup>1</sup> · Taohai Yan<sup>2</sup>

Received: 9 June 2023 / Revised: 12 August 2023 / Accepted: 16 August 2023 / Published online: 19 September 2023  
© The Author(s), under exclusive licence to the Korean Fiber Society 2023

## Abstract

Polyimide (PI) nanofiber membranes (NFMs) via electrospinning demonstrate widespread applications with an intrinsic drawback of lower mechanical performance, which could be improved with multi-wall carbon nanotubes (MWCNTs). PI NFMs was fabricated via a simple thermal induced imidization of polyamic acid (PAA) NFMs and MWCNTs/PI composite NFMs were also investigated on the effect of MWCNTs on morphology, mechanical performance, and its possible carbonization. Such simply thermal induced imidization of PAA demonstrates successfully to be PI, and small amounts of MWCNTs could reduce the diameter and distribution of MWCNTs/PI nanofibers, and coarse and granular-like surface appeared on MWCNTs/PI composite nanofibers as the MWCNTs was increased up to 1.0 wt.%. Notably, addition of MWCNTs improved thermal stability and mechanical performance of MWCNTs/PI composite NFMs, but it lowered the mechanical performance of such composite NFMs at higher carbonization temperatures, which makes its carbonized NFMs even more inclined to be fragile and fracture.

**Keywords** Electrospinning · MWCNTs · PI · Nanofiber membranes · Mechanical performance · Carbonization

## 1 Introduction

Electrospinning is the process of jet spinning a polymer solution or melt in a strong electric field. Under the action of an electric field as a critical voltage is reached, the surface tension of the polymer at spinneret tip is counter balanced by localized charges generated by the electrostatic force, then the droplets at the tip of the needle will change from spherical to conical (Taylor cone) and extend from the tip of the cone to obtain fibrous filaments [1]. In recent years, many different types of nanoscale fibers have been prepared through electrospinning or electrospun [2, 3], which is proved to be one of the most convenient, fast and effective, and a versatile and viable technique for generating ultrathin fibers [4]. Nanofibers from variable materials were the center of attention for industries and researchers due to their simplicity in manufacture and setup [3]. Among those,

polyimide (PI) is a kind of polymer with imide ring on the main chain possessing specific unique characteristics, such as higher density of aromatic ring on the molecular chain [5], good high and/or low temperature and radiation resistance, excellent mechanical properties, and good chemical stability [6]. As of those performances, PI is widely used in engineering plastics, high-temperature filtration, thermal protective clothing, adhesives, batteries, microelectronic devices, and high-value ones in certain fields [7–10].

The electrospun PI nanofiber membrane (NFMs) [11–13] has the advantages of large specific surface area, small pore size, and simple preparation process. As of that, such electrospun PI fiber materials have attracted more and more attention, which is accomplished by two ways via electrospinning technology. The first is by transforming polyimide acid (PAA) solution-based NFs through thermal imide treatment to PI solution, while the PAA solution is obtained by the synthesis of pyromellitic dianhydride (PMDA) with 4,4-diaminodiphenyl ether (ODA) as raw materials to prepare electrospun nanofibers. The inevitable shortcomings are the complexity of this synthesis process of PAA and the degradation phenomenon during the spinning process, as well as the problem of easy formation of micropores on the fiber surface and incomplete thermal amination [10,

✉ Taohai Yan  
thyan@mju.edu.cn

<sup>1</sup> School of Materials, Shanghai Dianji University, Shanghai 201306, China

<sup>2</sup> Fujian Key Laboratory of Novel Functional Fibers and Materials, Minjiang University, Fujian 350108, China

[13]. Due to the characteristic of PI with high solvent resistance, the second method is directly dissolving PI powder in organic solvents [11] as a proper solution for PI nanofibers electrospinning. This method is simple process, easy to apply and uniform surface of the as-prepared fibers, thus having been widely used into practices. For example, PI directly dissolved in organic solvent *N*-methyl-2-pyrrolidone (NMP) for obtaining exhibited smooth and hydrophobic surface NFMs for gas filtration. Alternatively, PI powder-based inks are directly electrospun into nanofibers acting as the surface layer of the fiber membrane improving the friction properties significantly [14]. However, the current electrospun PI nanofiber membrane has low strength of nanofibers and weak bonding points between fibers, resulting in NFMs exhibiting poor mechanical properties.

So far, quite a lot of attempts are explored and mostly used are nanofillers to enhance PI-based nanocomposites [15–17], and polyamide composite nanofibers through electrospinning also be of some help to address mechanical performance defects. For example, a toughened and self-healing carbon/epoxy composites using electrospun thermoplastic polyamide nanofibers as the matrix and found that this composite material can quickly and repeatedly repair damaged areas [18]. Christian Harito et al. electrospun and chemically converted the colloidal dispersion of titanate nanotubes and PAA in dimethylformamide (DMF) into PI–titanate nanotubes composite nanofibers with a diameter of 500–1000 nm, which improved the glass transition temperature of the composite materials [19]. In addition, a simple method to synthesize PI films by embedding part of imide PI/SiC nanofiber networks into PAA solutions has been proposed, which exhibits an enhanced dimensional stability, high mechanical properties, and optical transparency. In addition, compared with solution casted films, the self-filled PI films with nanofiber networks show excellent mechanical properties, high transparency retention rate, and much lower coefficient of thermal expansion [20]. Furthermore, rigid inorganic particle titanium dioxide has been explored to improve the mechanical strength of PI fiber membrane, and the chemical and thermal properties of PI fiber membrane are enhanced to a certain extent because of the excellent electrolyte wettability, acid–base property and thermal stability of titanium dioxide particles [21]. However, these preparation processes are relatively complex and difficult in the view of practical production.

Chemically speaking, PI has a regular rigid chain and an imide ring structure, with a carbon content of up to 70%. In addition, the aromatic heterocycles produce a conjugate effect, making the carbon accumulation in the carbonization process greater, which is conducive to the formation of graphite structure, and can be used as a good carbon precursor material [5]. Therefore, carbon nanotubes [22] could be used for enhance thermal and mechanical properties of

PI-based composites [17], due to the high strength, good conductivity and thermal conductivity, specifically multi-walled carbon nanotubes (MWCNTs) have been utilized to improve the mechanical properties of the fiber membrane [23–25] via composite electrospinning with polyamide acid to form a film. MWCNTs/PI were prepared by thermal amination, followed by carbonization to obtain MWCNTs/PI composite fiber carbonized films, leading to a mechanical properties and thermal stability improved MWCNTs/PI composite fiber membranes an compared that of pure PI fiber membranes [26, 27], which is enhanced by approximately 81% in tensile strength and 88% in Young's modulus of carbonized MWCNTs/PI composite fibers than pure PI fibers, respectively [28]. Besides, carbon fiber/polyimide (CF/PI) composite membrane has been prepared and found that PI, as a carbonization precursor, has high carbon conversion, good mechanical properties and thermal stability [29]. In addition, it was reported that the interface bonding performance of carbon fiber reinforced polyimide resin composite was poor, and a new surface treatment agent was designed and prepared to improve the interface strength by covalent bond between CF and PI matrix, thereby improving the mechanical properties of CF/PI composite to a certain extent [30]. All those together implied carbon-based materials, especially MWCNTs, could be of great help to improve the mechanical and thermal properties of polymeric nanofibers.

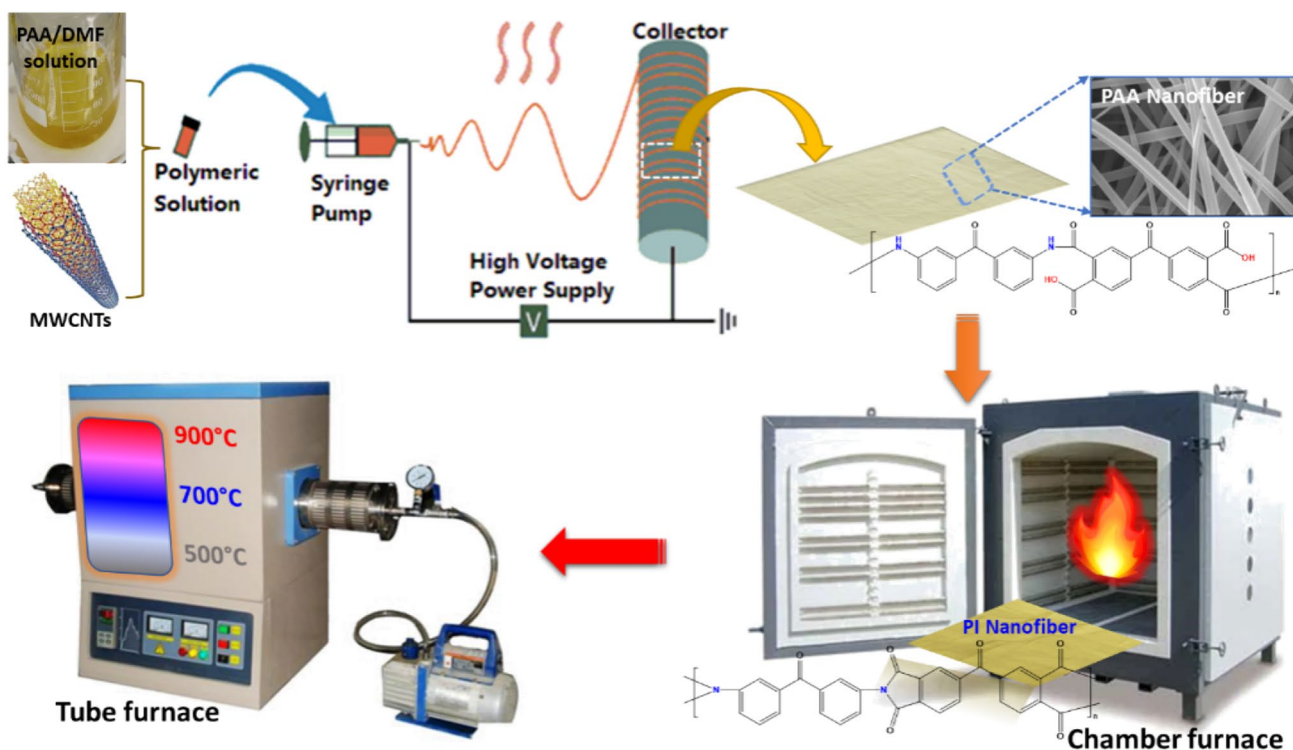
In this study, polyimide (PI) nanofiber membranes (NFMs) were prepared by the simple thermally induced imide reaction of electrospun polyamide acid (PAA) NFMs and tried to use MWCNTs as additives to improve the mechanical properties of PI NFMs. Herein, the effects of MWCNTs loading amount on its PI-based composite NFMs regarding the morphology, mechanical properties, and possible carbonization process of MWCNTs were studied for possible applications requiring high-temperature resistance and maintaining some mechanical support.

## 2 Experiment

### 2.1 Materials

A 15 wt.% polyamic acid solution in DMF (PAA, Jiangsu Teyue Plastic Ltd., Co.) was used as the precursor for polyimide (PI) synthesis. Multi-wall carbon nanotubes (MWCNTs, outer diameter is about 5–25 nm, average length via is 2.5  $\mu\text{m}$ , and the specific surface area is  $\sim 300 \pm 25 \text{ m}^2/\text{g}$ ) was used as additives and purchased from Knorth Technology Ltd., Co.

The electrospinning platform was assembled in-house using these three major units, including a high voltage direct current power supply (DW-P303-1ACDF0, Hengbo Power



**Scheme 1** Procedure of fabricating PAA, PI and its corresponding carbonized nanofiber membrane

Ltd., Co.), reciprocating motion platform and low-speed collection drum (Benning Electrospinning Equipment Ltd., Co.), and high-precision micro dual channel electrospinning syringe pump (Dylan Electrical Technology Ltd., Co.).

Chamber resistance furnace (SX2-4-10A, Shaoxing Shangyu Daoxu Kexi Equipment Company, Zhejiang, China) for imidization of PAA upon heating. Tube furnace (TF/200-40S, Shanghai Micro-X Furnace Ltd., Co.) for carbonization was carried out under vacuum at different temperatures.

## 2.2 Electrospinning Fabricated Nanofiber Membranes

The procedure of PAA, PI and its corresponding carbonized nanofiber membrane is briefly illustrated in Scheme 1. First, the PAA solution and its corresponding electrospinning nanofiber membrane is prepared as the following. Certain amounts of MWCNTs powder were added to the solution of 15 wt.% PAA in DMF, as the weight of MWCNTs based on PAA is 0.1 wt.%, 0.5 wt.% and 1.0 wt.%, and a homogeneous MWCNTs/PAA solution in DMF was obtained via mechanical stirring at ambient for 24 h, which is ready for the electrospinning for PAA and MWCNTs/PAA nanofiber membranes.

After several trials, the parameters for electrospinning were carried out at voltage of 18 kV running for 20 h, and

the solution flow rate is adjusted to be 0.2 mL/h with the gauge between syringe tip and the collection drum is 18 cm, and the rotating speed of collection drum is 110 rpm. The PAA nanofiber membranes with varied loading amount of MWCNTs were obtained for further experiments.

Polyimide (PI) is produced by imidization of polyamic acid (PAA) through the dehydration in air under thermal treatment [31, 32]. Hereby, in the chamber resistance furnace with being preheated to 100 °C, PAA and MWCNTs/PAA composite nanofiber membranes under imidization upon heating were conducted with the chamber with a heating rate of 5 °C/min and holding at 100 °C for 1 h followed by to 200 °C and holding for 1 h, continues to 250 °C and maintain the temperature for 30 min and followed by further heating up to 300 °C with a isothermal for 1 h [33]. Then, cooling down to room temperature naturally and samples are labeled as PI and MWCNTs/PI composite nanofiber membranes and ready for characterization.

The as-prepared PI and MWCNTs/PI composite nanofiber membranes were under carbonization process, which is conducted in the tube furnace under vacuum. After the nanofiber membranes was placed in position, a pretreatment is heating at 5 °C/min to 400 °C and maintained for another hour, and then carbonization starts at different temperatures (500 °C, 600 °C, 700 °C, 800 °C, 900 °C and 1000 °C) for 1 h rises from 400 °C. Afterwards, the tube furnace was cooled down to room temperature naturally.

## 2.3 Characterization

The surface morphology of nanofiber membranes was carried out using scanning emission microscopy (SEM, Hitachi S-4800, Japan) under an accelerated voltage of 2 kV after the gold plate sputter coating, and the diameter and its distribution of nanofiber was measured by the associate software and counted up to 100 for the fineness measurement.

Attenuated total refraction Fourier Transform Infrared Spectrometer (ATR FTIR Spectrometer, IRAffinity-1S, SHIMADZU) was explored for the chemical structure analysis of as-spun PAA and its corresponding PI nanofiber membranes in the range of 4000–400  $\text{cm}^{-1}$  with averaging 16 scans under a resolution of 4  $\text{cm}^{-1}$ .

Thermogravimetric Analysis (TGA, TG209 F1, Netzsch, Germany) was used for evaluating thermal stability of all the nanofiber membranes and the corresponding carbonized one from room temperature to 900  $^{\circ}\text{C}$  with a heating rate of 10  $^{\circ}\text{C}/\text{min}$  under argon atmosphere of 50 mL/min.

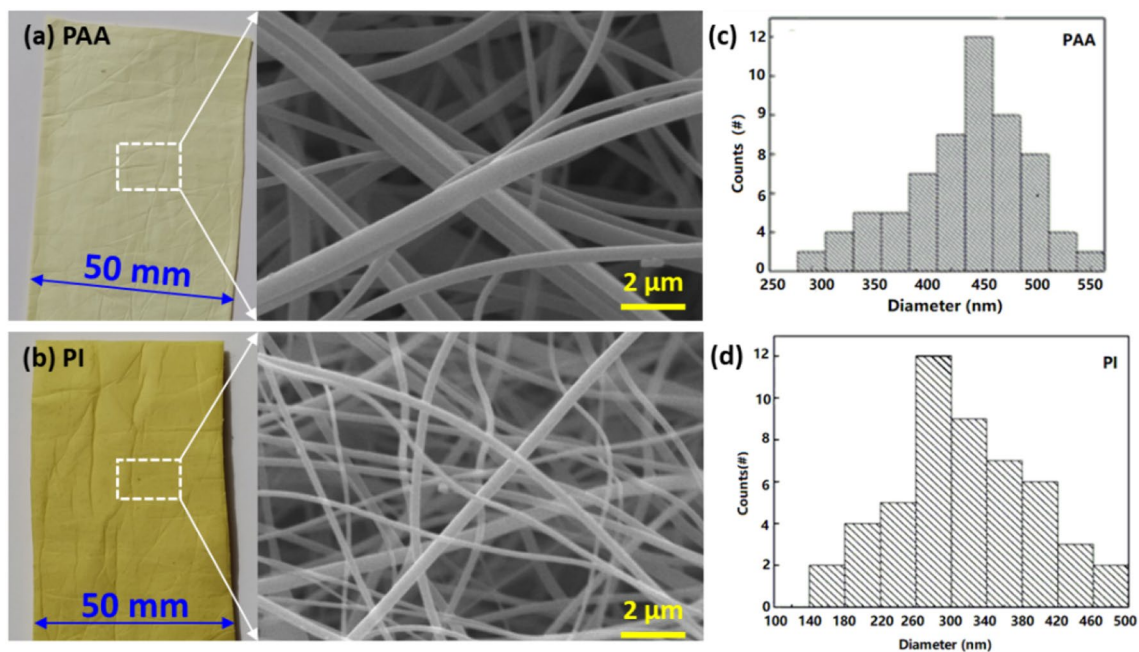
Universal material testing system of Instron<sup>®</sup> 3400 was applied on the mechanical performance evaluation of all the PI nanofiber membranes under ambient conditions with a fixed elongation rate of 20 mm/min with a sample gauge of 160 mm. The as-spun nanofiber membrane was cut into 20 mm in width by 200 mm in length, and the load–displacement curves for comparison were reported.

## 3 Results and Discussion

### 3.1 Membranes Surface Morphology Analysis

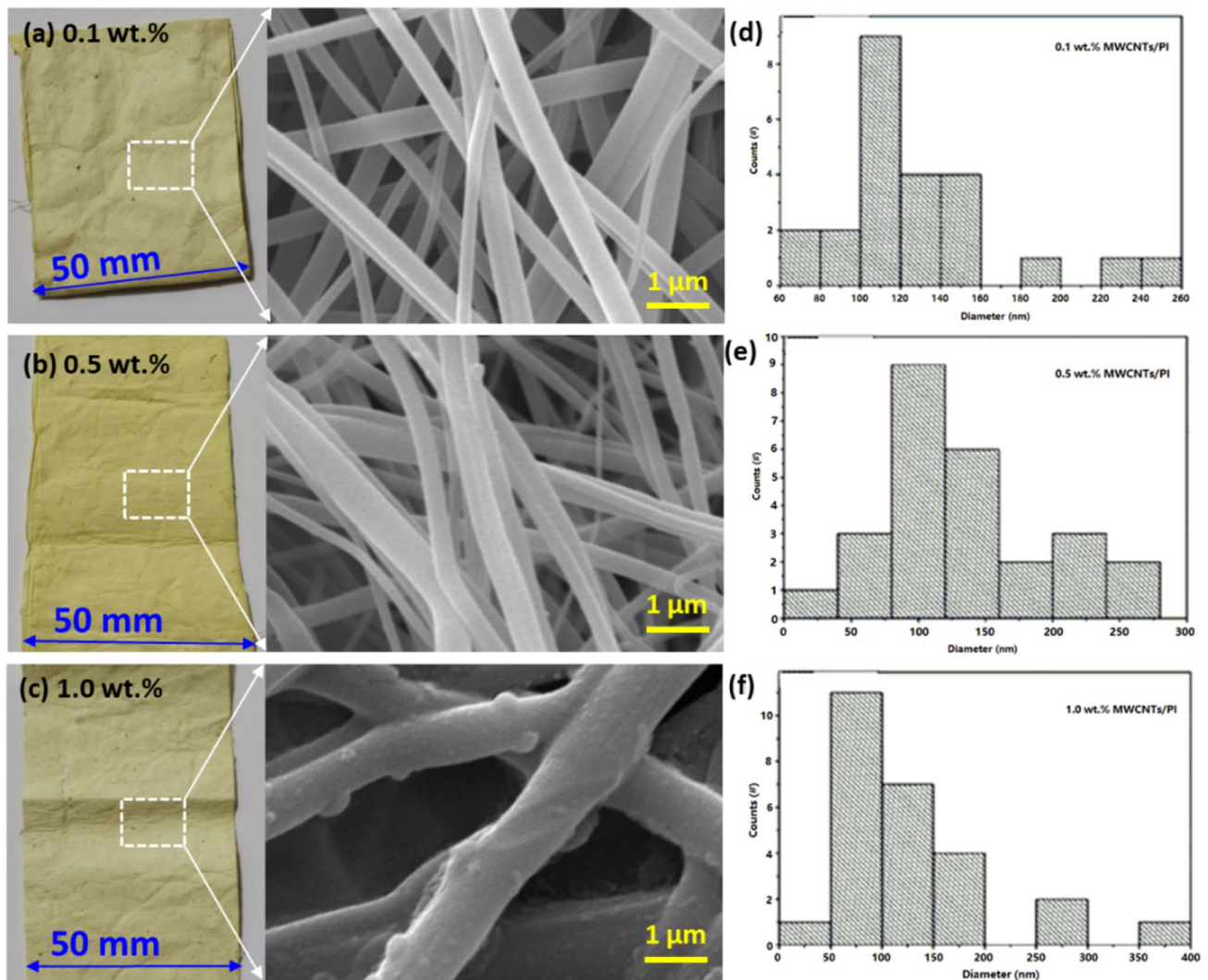
Figure 1 demonstrates the appearance and surface morphology of PAA and PI NFMs and the SEM images are used for the fiber diameter measurement, and Fig. 1a is for the PAA NFM and Fig. 1b shows the PI one after thermal induced imidization of PAA in chamber furnace at desired temperature for required period. The color difference between the two figures is obvious. The PI nanofiber membrane after high temperature treatment is yellowish, while the PAA nanofiber membrane is light in color. As can be seen from Fig. 1c that the diameter distribution of as-spun PAA nanofibers is from 275 to 575 nm with an average one of 426 nm, while that of PI nanofiber after imidization is of 315 nm averaged from 140 to 500 nm in Fig. 1d. Overall, PI nanofiber is significantly thinner by 111 nm in average than its precursor PAA ones, and that could be ascribed to the evaporation of DMF solvent residue induced shrinkage combined with polycondensation releasing small molecules such as water during the imidization process, the latter of which seems contributed more, since two water molecules come along with such imidization.

Figure 2 manifests the optical appearance and surface morphology of MWCNTs/PI composite NFMs with different loading amounts of MWCNTS, and its corresponding nanofiber diameter distribution. As the loading amount of



**Fig. 1** Observation photos, SEM images and fiber diameter distribution of the as-made (a, c) PAA and b, d PI electrospinning NFMs





**Fig. 2** Observation photos, SEM images and fiber diameter distribution of MWCNTs/PI composite NFMs with varied MWCNTs loading amount: **a, d** 0.1 wt.%, **b, e** 0.5 wt.% and **c, f** 1.0 wt.%

MWCNTs is 0.1 wt.%, all the nanofibers possess a quite smooth surface with less variation in shape and diameter as back up by Fig. 1a, d. As the MWCNTs loaded up to 0.5 wt.%, there are many noticeable tiny beads-like irregular on the surface of nanofiber along its longitude direction, leading to some kind of twist or bend here and there and exhibiting larger differences in the nanofiber diameter distribution as illustrated in Fig. 2e. As further increase MWCNTs amount of 1.0 wt.%, much more granules and small beads-like emerged on the surface of nanofibers, making the surface no longer smooth, frankly speaking the surface is quite coarse and even some unexpected to be irregular-shaped nanofibers as perceived in Fig. 2c, and in diameter distribution is even larger from 50 to 400 nm than that in nanofibers with MWCNTs of 0.1 wt.% (Fig. 2f). Such quite coarse surface of 1.0 wt.% MWCNTs/PI nanofiber,

especially those surface area attached big granular are highly possible due to the self-aggregation of MWCNTs from the solution/dispersion making step, which is unlikely to be seen or noticed by naked eyes at that time. However, these MWCNTs/PI composite nanofiber with such coarse surface with overloaded MWCNTs could exhibit some tradeoff between the specific surface area and the diameter of the resulted nanofibers, which might also change the porosity distribution of this type of PI-based composite NFMs, and other functionalities might of further interesting to be pursued in the future.

Figure 3 exhibits the optical photos and SEM images of 0.5 wt.% MWCNTs/PI composite NFM before and after carbonization. As the color change from yellow to black suggests the some chemical reaction happened at the temperature of 500 °C and above. Besides, as can be seen from

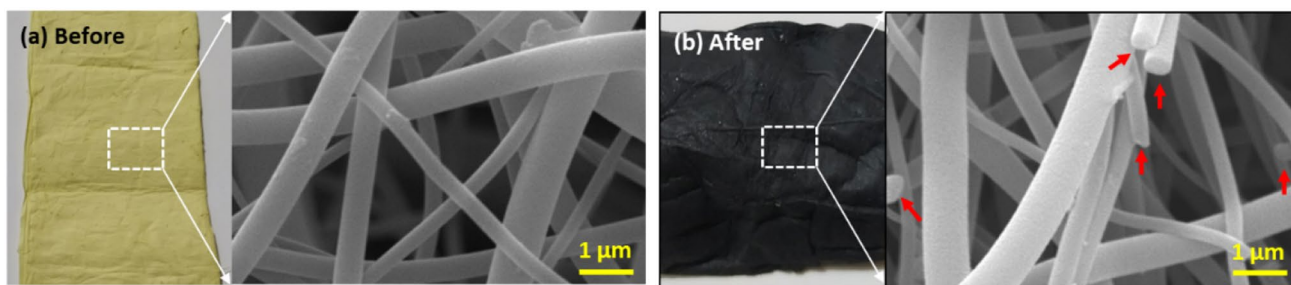


**Fig. 3** Optical photos and SEM images of 0.5 wt.% MWCNTs/PI composite NFM **a** before and **b** after carbonization in tube furnace

Fig. 3b that much more nanofibers with broken cross sections were noticed and observed as compared to that in Fig. 3a of nanofiber before carbonization. The most likely possible reason is the linamide bonds in PI also broken during such carbonization process resulting in the fragile of nanofiber in carbonized membranes (as indicated by red arrows in SEM image of Fig. 3b), and such carbonized fiber length reduce happened in carbon fiber production and might be due to the high-temperature activation that contributes to the removal of the volatile low molecular weight fractions [34], which also leading to some the thermal residual stress upon heat treatment type carbonization that may affect the strength of fiber, fiber damage and eventually failure of the continues fiber morphology-like broken structure. This is also felt a little bit lighter by transferring the carbonized membranes out of the tube furnace and some black debris was noticed left in the sample holding boat.

### 3.2 Structure Analysis on Imidization Reaction

We were trying to minimize the possible energy for thermal induced imidization of converting PAA to be PI [35], and the temperature are key to affect the structural and properties [36–38], such as physico-chemical, mechanical, thermal [39] and electrical properties of such PI [40, 41]. Herein, thermally imidization was starting and holding at 200 °C for 1 h in chamber furnace, and FTIR spectrum, as shown in Fig. 4 that only partial imidization was achieved resulting a PAA/PI composite with the characteristics FTIR bands at both 1716 cm<sup>-1</sup> and 1665 cm<sup>-1</sup> comes from PAA with a new peak at 1370 cm<sup>-1</sup> ascribed to PI. Then, further increase the temperature just up to 300 °C, interestingly as noted in Fig. 5 that

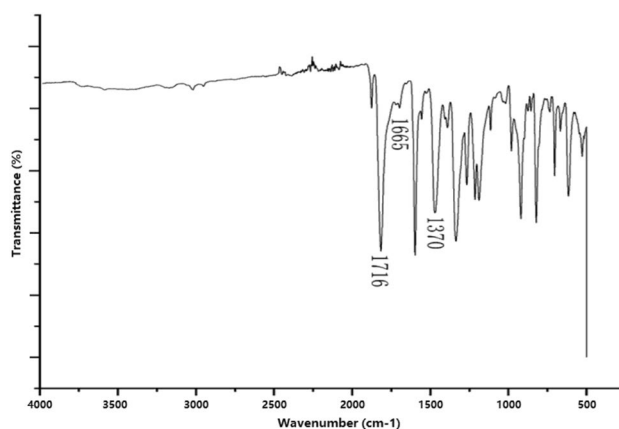


**Fig. 4** FTIR spectrum of PI NFM via partial imidization of PAA at 200 °C

new FTIR peaks at 1774 cm<sup>-1</sup> and significantly increased at 1722 cm<sup>-1</sup> with vanished ones at 1712, 1644 and 1539 cm<sup>-1</sup>, indicating the cyclization between the carboxylic acid group and its adjacent amide and PAA was fully converted to be PI. Furthermore, the peaks of 1774 and 1722 cm<sup>-1</sup> are assigned to C–O asymmetric stretching, and the sharp one at 1370 cm<sup>-1</sup> is belong to the C–N bond, suggesting the show-up of new imide functional group. Then, the imidization reaction could be accomplished at 300 °C, and even higher one could also lead to the imidization, but it would come along with some degree of carbonization leading to darken the color of nanofiber membrane and increases the brittleness, which is better to be avoided as much as possible to minimize the potential surface carbonization and possible oxidation [42]. The PAA is thermally or chemically converted into PI through dehydration and cyclization reactions as Eq. (1).

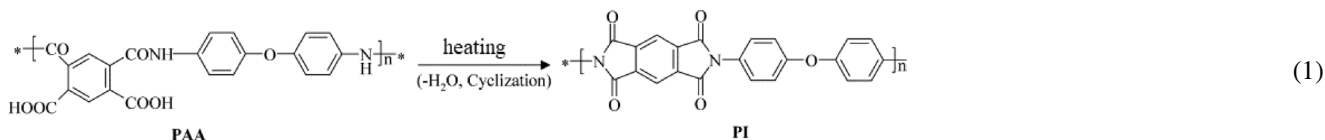


**Fig. 5** FTIR spectrum of PAA and PI NFM via imidization of PAA @ 300 °C

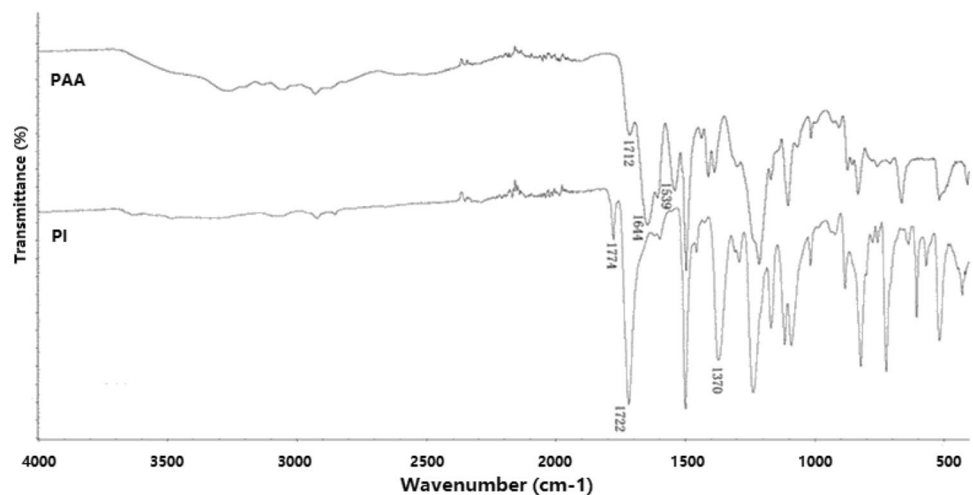
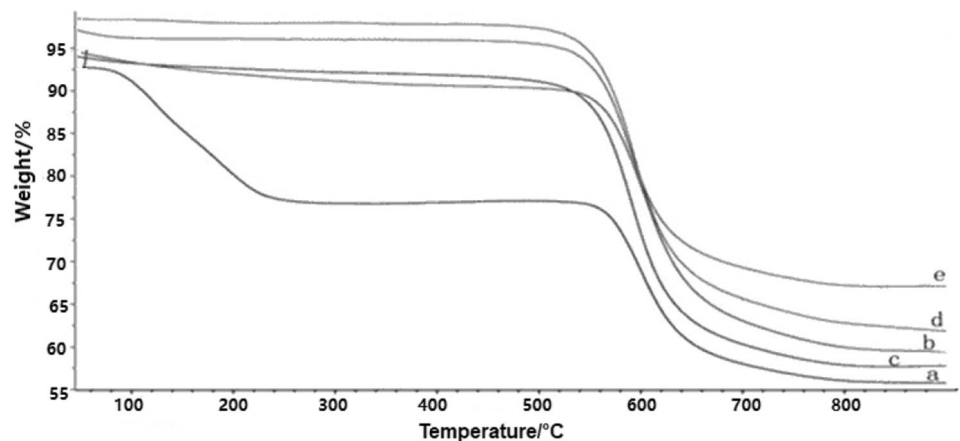


**Fig. 6** TG traces of **a** PAA and MWCNTs/PI composite NFMs with varied loading amount of MWCNTs: **b** 0.0 wt.%, **c** 0.1 wt.%, **d** 0.5 wt.% and **e** 1.0 wt.%



### 3.3 MWCNTs/PI Composite NFMs Analysis

#### 3.3.1 Thermal Stability Analysis

The thermal stability evaluation of all the NFMs via TGA under argon atmosphere are shown in Fig. 6. As can be implied from Fig. 6a is that thermal stability profile of PAA exhibits two thermal decomposition phases, which is the precursor of PI, and the first continuous one in the temperature range of 90 to 240 °C is most like the evaporation of solvent DMF residue, since the major component weight of DMF is around 85 wt.% and its boiling point is about 153 °C. As the temperature further increases and approaching to 280 °C, there is no more weight loss forming a plateau with barely noticeable slope, indicates the imidization of converting PAA to PI was occurring and finished around 540 °C. This could be regarded as circumstantial evidence for the partial imidization as manifested by FTIR spectrum, as illustrated in Fig. 4, and it also likely to recommend doing the imidization at least at 300 °C as backed up by the FTIR data in Fig. 5.

**Table 1** Thermal properties of PI composite NFMs with varied amount of MWCNTs

TGA sample	MWC-NTs/wt.%	*T <sub>5%</sub> /°C	*T <sub>10%</sub> /°C	Residue mass@900C/wt.%
b	0.0	500	573	53.42
c	0.1	473	553	51.65
d	0.5	519	575	56.71
e	1.0	578	593	62.12

\*Note: T<sub>5%</sub> and T<sub>10%</sub> are stand for the temperature that about 5 wt.% and 10 wt.% weight loss occurred, respectively

On the other hand, Fig. 6b–e shows thermal decomposition profiles of PI-based composite NFMs with varied loading amount of MWCNTs, and key thermal evaluation parameters are summarized in Table 1. All thermal profiles of MWCNTs/PI composite NFMs are in the very similar pattern [43], regardless of MWCNTs loading amount. In addition, there is only a tiny amount of weight loss around 3–6% in the MWCNTs/PI composite NFMs in the temperature

range of 100 °C through 300 °C, which might be the reason the drain out the tiny residue of DMF solvent in such porous membranes and partially thermal decomposition of functional group such as hydroxyl and carboxylic acid on the surface of the MWCNTs explored. In addition, the major thermal decomposition for all the MWCNTs/PI composite NFMs are in the temperature range of 550 to 850 °C, leaving roughly of 57.5 wt.% residue for loading 0.5 wt.% MWCNTs and about 68 wt.% residue for MWCNTs amount of 1.0 wt.%.

Specifically, MWCNTs amount of 0.1 wt.% in the PI composite nanofiber membranes, its  $T_{5\%}$  and  $T_{10\%}$  points are both lower by 27 °C than that of pure PI one, and less by about 2.1wt.% residue mass at 900 °C, as listed in Table 1, which might because of lower amount of MWCNTs is insufficient to improve the thermal stability of PI nanofiber membrane[44], and possibly the addition of such tiny MWCNTs could deteriorate the PI molecular aligned aggregates resulting from the localized pi-pi stacking between its aromatic rings, since the longer MWCNTs could break those alignments and further worsen its aggregations and bonding between PI molecular, thus weaken the thermal stability and accelerate thermal decomposition of such 0.1 wt.% MWCNTs/PI composite nanofiber membranes. Further continuously increases the amount of added MWCNTs up to 0.5 wt.% and 1.0 wt.%, the corresponding  $T_{5\%}$  and  $T_{10\%}$  points are even higher than that of PI membrane, and so does for the residue mass at 900 °C (Table 1).

All those together implies that higher addition of MWCNTs improves thermal stability of its PI composite NFMs. There might be two possible reasons. As more MWCNTs was added into the PI matrix, each one of MWCNTs could offer as a molecular anchor joint and in total would be quite a lot such joints through the PI matrix [45], as such restraint the PI molecular vibrations upon heating, leading to more

thermal energy is needed to start the decomposition of PI, and then the thermal stability of MWCNTs/PI composite NFMs is enhanced. In addition, another one is that the thermal conductivity of MWCNTs is much higher than that of PI matrix, and inherited even greater thermal stability, and more MWCNTs could forming a percolation network through the PI matrix and conduct the heat out of PI matrix, lower the temperature of PI molecules at least those adjacent to the MWCNTs and reduce the thermal accumulation rate among the PI molecules, which is kind of way to keep PI matrix from thermal decomposition upon heating and further strengthening the thermal stability of MWCNTs/PI composite nanofiber membranes.

### 3.3.2 Mechanical Behavior and Performance Analysis

Here, load–displacement curve measures the extrinsic properties of a specimen (ultimate load, yield points, and possible energy absorbing performance) [46, 47] under varied mechanical testing [48] as shown in Fig. 7a, and the main parameters are stiffness, work to failure as highlighted in the shaded area, and ultimate load and displacement, which is not the same as that of stress–strain curve that is usually normalized for the sample dimensions. The tensile evaluation of MWCNTs/PI composite NFMs with varied loading amount of MWCNTs are exhibited in Fig. 7b. Initially without any MWCNTs as noted of 0.0 wt.% curve, that is the pure PI NFM, the load is continuously increasing slowly as the displacement goes at the rate of 20 mm/min till it reach the ultimate load without any noticeable yield point as usually observed and followed by the broken quickly in about 1 min. As the addition of MWCNTs is 0.1 wt.%, there is a clearly linear region within the displacement of 40 mm, which suggests a clear improvement in the stiffness, and a noticeable yield point along with a higher ultimate load as mostly ascribed to even such tiny amount of

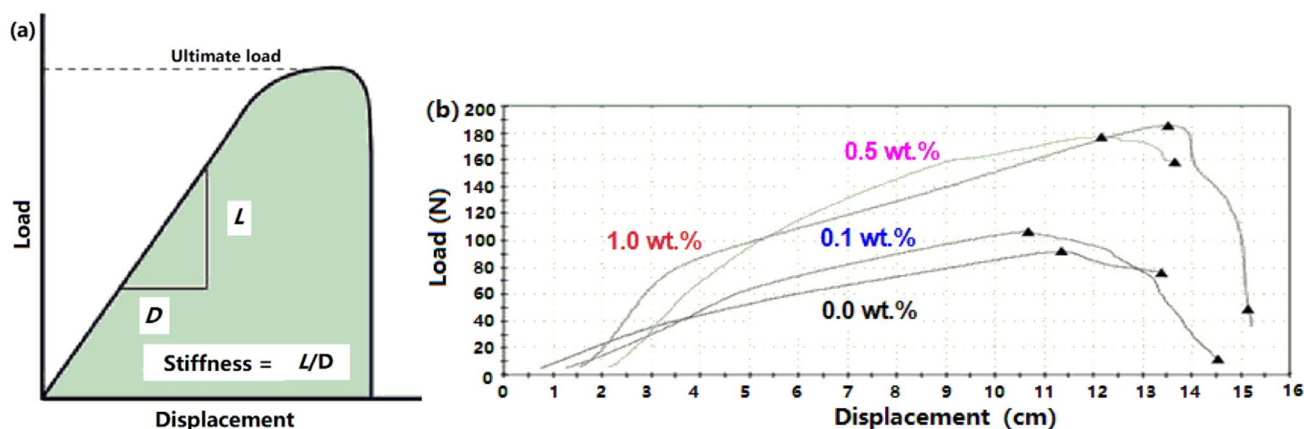


**Fig. 7** a Load–displacement curves of b MWCNTs/PI composite NFMs with varied loading amount of MWCNTs: 0.0 wt.%, 0.1 wt.%, 0.5 wt.% and 1.0 wt.%



MWCNTs and then goes to a region that is kind of parallel to that without MWCNTs, and lastly reaches to the broken with longer elongation ratio through a bumpy process in about 2 min (curve noted as 0.1 wt.%). As the MWCNTs further increased up to 0.5 wt.%, a quite enhancement in the stiffness is observed with a clearer yield point, increased breaking strength and elongation at break are almost twice as that of pure PI NFM, as indicated from Table 2. As similar increase in the stiffness was noticed as the MWCNTs increased to be 1.0 wt.%, but the ultimate load and strength is as close as that of 0.5 wt.% MWCNTs/PI composite NFM (Table 2), but exhibit an even quick bumpy broken process as compared to the rest of the composite NFMs. The common could derived from Fig. 7b is that the mechanical performance, such as ultimate load, stiffness, strength, and elongation, of MWCNTs/PI NFMs are improved with the addition of MWCNTs due to the intrinsic higher strength and larger length/diameter ratio of MWCNTs as additives.

Besides, the higher specific surface area of MWCNTs providing much more anchor area with PAA and/or PI matrix [49], and the newly formed interphase and improves interfacial adhesion between the surface of MWCNTs and PI matrix would contribute to enhance the mechanical performance of its composite NFMs. However, the improvements and enhancements on the interphase and interfacial adhesion are greatly influenced by the homogeneously distribution of MWCNTs through the whole PI matrix, especially in the precursor PAA ones that involving the processing of MWCNTs suspension and electrospinning parameters that deserved a further consideration. Since there is always a self-aggregation of CNTs [50], which makes even harder to get uniform size distribution of nanofiber, and such aggregation could also bring some cavity or void in the perimeter or interphase adjacent to the polymeric matrix, which could cause a stress concentration before the extra load was applied and then deteriorate the mechanical performance of composite NFMs as expected.

### 3.4 Carbonization Analysis of PI and MWCNTs/PI Composite NFMs

In the process of carbonizing polyimide to prepare carbon films at different temperatures in the absence of oxygen,

**Table 2** Mechanical properties of PI composite NFMs with varied amount of MWCNTs

MWCNTs/wt.%	Breaking strength/MPa	Elongation at break/%
0.0	3.69	37.47
0.1	4.28	43.57
0.5	7.42	76.76
1.0	7.10	64.97

alternatively named pyrolysis by thermally induced chemical decomposition of organic materials, carbonization temperature is the key to the structural modification of the films [51] for certain functionalities and applications [52]. PI and its MWCNTs/PI composite NFMs are quite thermally stable in the range of 350 through 550 °C as indicated by the TGA traces shown in Fig. 6. That suggests PI is highly capable of affording thermal treatments under 550 °C without any properties being affected [53]. Hereby, the carbonization process of 0.5 wt.% MWCNTs/PI composite NFMs was set as an example of probing the effect of carbonization on the mechanical performance with the temperatures carried out at temperature higher than 550 °C, at least of 600 °C, which is summarized in Fig. 8 and Table 3.

As can be implied from Fig. 8 that the strength and elongation at break decreased significantly as the carbonization temperature increases, which is supported by the fragile observation of the carbonized NFMs as the SEM indicated in Fig. 3b. In addition, the load reached its minimum at the carbonization temperature continues increase up to 800 °C, and then increased up to the highest at 900 °C for carbonization followed by a close load at 1000 °C as that of carbonization

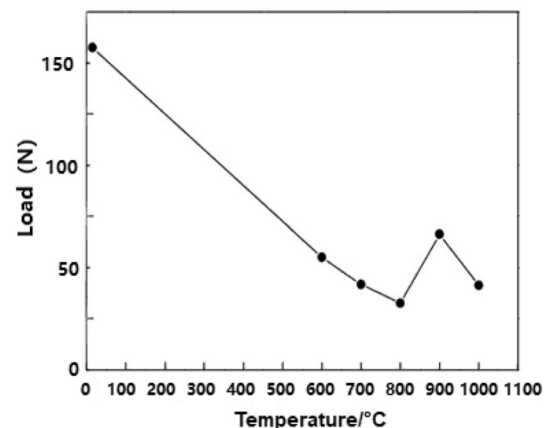


**Fig. 8** Max load of 0.5 wt.% MWCNTs/PI composite NFMs under different carbonization temperatures

**Table 3** Mechanical properties of 0.5 wt.% MWCNTs/PI composite NFMs at different carbonization temperatures

Temperature/°C	Breaking strength/MPa	Elongation at break/%
0	7.42	76.76
600	4.71	13.87
700	3.56	10.31
800	2.63	7.54
900	3.74	7.73
1000	3.15	6.12

at 700 °C. This observation on the sharp change at 800 °C also matches the barely changes in weight loss at 800 °C in the TGA traces as exhibited in Fig. 6, which could be the implication that the carbonization could be done at 800 °C for 1 h with a completely done on the interior gas phase out and new C–C bond formation. At such carbonization temperature of 800 °C, along with the emission of various small molecules [54], the process of carbon microcrystalline have been formed or organized in order as supposed to be lower orientation, and increase micropores, cavities and disorder in the carbonized NFM leading to the changes in or worst mechanical performance [55].

On the other hand, at a higher temperature of 900 °C for further carbonization [56, 57], it is possible that the disorder results from carbonization at lower temperature would be improved and transfer to be a status with more carbon microcrystals with higher orientation and packing closely with adjacent ones, plus some decomposition residue from PI at 900 °C serves as plasticizer bonding those carbonized microcrystal regions and this shows noticeable improvement in mechanical performance, as listed in Table 3. However, as the carbonization temperature reaches to 1000 °C, decomposition residue from PI at lower temperature would further being carbonized forming gas phase out of the matrix, which could leave more cavities, microcracks and micropores, and thus lowered the mechanical performance of the carbonized NFMs. This result also reached a similar conclusion in Yang's research, where the carbonization yield monotonically decreased from 64% at 700 °C to 53% at 1000 °C [58].

## 4 Conclusions

The polyimide (PI) nanofiber membrane prepared by electrospinning has the characteristics of large specific surface area and small pore size, which has potential application value in the fields of battery separation film and microelectronic devices. In this paper, electrospun PAA nanofiber membranes (NFMs) were prepared using polyamic acid (PAA) solution as precursor, and then converted into PI nanofibers by thermally induced imidization treatment, and the chemical structure via FTIR of PI and PAA NFMs confirmed that PAA NFMs were successfully imidized into be PI ones as expected. Then, multi-walled carbon nanotubes (MWCNTs) were added in the electrospinning process for enhancing the thermal and mechanical performances of PI-based composites NFMs. It turns out that a small amount of addition can reduce the fiber diameter, but it is easy to cause agglomeration when the addition amount is too much, resulting in larger fiber diameter and coarse bulging surface. The increase of MWCNTs content is beneficial to improve the thermal stability of MWCNTs/PI composite NFMs, resulting in gradually increase in the stiffness, the breaking strength

and elongation at break. In addition, after the carbonization of 0.5 wt.% MWCNTs/PI composite NFMs at high temperature above 600 °C, while the fracture strength and elongation decreased significantly with the carbonization progress, but details in kinetic changes is not clear so far, which is worth to be investigation in the future for expanding the MWCNTs/PI composites and its carbonized NFMs in other possible realms of requiring an enhanced the thermal stability, mechanical properties and longer durability simultaneously, such as high-value products, such as ultrafiltration, high-energy density battery separator and microelectronic devices.

**Funding** China Scholarship Council, 202008350058, Taohai Yan, Fujian Science and Technology Project Guidance Project, 2022H0049, Taohai Yan, Fuzhou Science and Technology Major Project, 2021-Z-3, Taohai Yan, The 2020 Shanghai Higher Education Teacher Training Plan of Shanghai Municipal Education Commission Teacher Professional Development Project.

**Data Availability** The authors declare that the data supporting the findings of this study are available within the paper. Should any raw data files be needed in another format they are available from the corresponding author [T. Yan] upon reasonable request.

## Declarations

**Conflict of Interest** The authors declare no competing financial interests.

## References

1. J. Stanger, N. Tucker, K. Kirwan, M.P. Staiger, Effect of charge density on the Taylor cone in electrospinning. *Int. J. Modern Phys. B* **23**(7), 1956–1961 (2009)
2. A. Nadaf, A. Gupta, N. Hasan, S. Fauziya, P. Ahmad, F.J.A. Kesharwani, Recent update on electrospinning and electrospun nanofibers: current trends and their applications. *RSC Adv.* **12**(37), 23808–23828 (2022)
3. J. Xue, T. Wu, Y. Dai, Y. Xia, Electrospinning and electrospun nanofibers: methods, materials, and applications. *Chem. Rev.* **119**(8), 5298–5415 (2019)
4. H. Vahabi, H. Wu, M.R. Saeb, J.H. Koo, S. Ramakrishna, Electrospinning for developing flame retardant polymer materials: Current status and future perspectives. *Polymer* **217**, 123466 (2021)
5. R. Ishige, C.L. Song, S. Hara, S. Ando, S.G. Kazarian, Analysis of spatial orientation distribution of highly oriented polyimide film using micro ATR-FTIR spectroscopic imaging method. *Polymer* **221**, 123616 (2021)
6. R. Yuan, Y. Zhou, X. Fan, Q. Lu, Negative-poisson-ratio polyimide aerogel fabricated by tridirectional freezing for high- and low-temperature and impact-resistant applications. *Chem. Eng. J.* **433**, 134404 (2022)
7. Y.-Y. Liu, Y.-K. Wang, D.-Y. Wu, Synthetic strategies for highly transparent and colorless polyimide film. *J. Appl. Polym. Sci.* **139**(28), e52604 (2022)
8. R. Khazaka, M.L. Locatelli, S. Diahm, P. Bidan, Endurance of thin insulation polyimide films for high-temperature power module applications. *IEEE Transact. Comp. Packag. Manuf. Technol.* **3**(5), 811–817 (2013)

9. S. Mandal, G. Song, An empirical analysis of thermal protective performance of fabrics used in protective clothing. *Ann. Occup. Hyg.* **58**(8), 1065–1077 (2014)
10. Y. Wang, M. Shang, Y. Wang, B. Cui, Z. Qiu, H. Li, Y. Wang, Polyimide composite films reinforced by graphene quantum dots. *Fullerenes, Nanotubes, Carbon Nanostruct.* **30**(6), 683–691 (2022)
11. G. Sun, G. Dong, L. Kong, X. Yan, G. Tian, S. Qi, D. Wu, Robust polyimide nanofibrous membrane with porous-layer-coated morphology by in situ self-bonding and micro-crosslinking for lithium-ion battery separator. *Nanoscale* **10**(47), 22439–22447 (2018)
12. B. Yi, Y. Zhao, E. Tian, J. Li, Y. Ren, High-performance polyimide nanofiber membranes prepared by electrospinning. *High Perform. Polym.* **31**(4), 438–448 (2018)
13. A.K. Gautam, C. Lai, H. Fong, T.J. Menkhous, Electrospun polyimide nanofiber membranes for high flux and low fouling microfiltration applications. *J. Membr. Sci.* **466**, 142–150 (2014)
14. Y. Kim, X. Wu, J.H. Oh, Fabrication of triboelectric nanogenerators based on electrospun polyimide nanofibers membrane. *Sci. Rep.* **10**(1), 2742 (2020)
15. V.E. Ogbonna, A.P.I. Popoola, O.M. Popoola, S.O. Adeosun, A review on polyimide reinforced nanocomposites for mechanical, thermal, and electrical insulation application: challenges and recommendations for future improvement. *Polym. Bull.* **79**(1), 663–695 (2022)
16. T.D. Mekuria, T.A. Wogsato, Synthesis, characterization and properties of polyimide nanocomposite thin films reinforced with TiO<sub>2</sub>/Al<sub>2</sub>O<sub>3</sub> hybrid nanoparticles. *Mater. Today Commun.* **32**, 103903 (2022)
17. Z. Wu, J. Dong, C. Teng, X. Li, X. Zhao, X. Qin, C. Ji, Q. Zhang, Polyimide-based composites reinforced by carbon nanotube-grafted carbon fiber for improved thermal conductivity and mechanical property. *Comp. Communicat.* **39**, 101543 (2023)
18. B. Chen, H. Cai, C. Mao, Y. Gan, Y. Wei, Toughening and rapid self-healing for carbon fiber/epoxy composites based on electrospinning thermoplastic polyamide nanofiber. *Polym. Compos.* **43**(5), 3124–3135 (2022)
19. C. Harito, R. Porras, D.V. Bavykin, F.C. Walsh, Electrospinning of in situ and ex situ synthesized polyimide composites reinforced by titanate nanotubes. *J. Appl. Polym. Sci.* **134**(13), 44641 (2017)
20. F. Liu, Z. Liu, S. Gao, Q. You, L. Zou, J. Chen, J. Liu, X. Liu, Polyimide film with low thermal expansion and high transparency by self-enhancement of polyimide/SiC nanofibers net. *RSC Adv.* **8**(34), 19034–19040 (2018)
21. W.-C. Liaw, Y.-L. Cheng, Y.-S. Liao, C.-S. Chen, S.-M. Lai, Complementary functionality of SiO<sub>2</sub> and TiO<sub>2</sub> in polyimide/silicitanita ternary hybrid nanocomposites. *Polym. J.* **43**(3), 249–257 (2011)
22. N. Anzar, R. Hasan, M. Tyagi, N. Yadav, J. Narang, Carbon nanotube—a review on synthesis, properties and plethora of applications in the field of biomedical science. *Sens. Int.* **1**, 100003 (2020)
23. B. Peng, M. Locascio, P. Zapol, S. Li, S.L. Mielke, G.C. Schatz, H.D. Espinosa, Measurements of near-ultimate strength for multiwalled carbon nanotubes and irradiation-induced crosslinking improvements. *Nat. Nanotechnol.* **3**(10), 626–631 (2008)
24. D. Zhai, H. Zhao, Z. Gao, Y. Guo, Q. Li, G. Wang, G. Zhao, Surface treatment of multiwalled carbon nanotubes and the formation of the multiscale conductivity network in long carbon fiber reinforced polypropylene. *Polym. Compos.* **43**(7), 4645–4659 (2022)
25. H. Bian, J. Xue, G. Hao, Y. Hao, M. Xie, C. Wang, Z. Wang, L. Zhu, Y. Xiao, High thermal conductivity graphene oxide/carbon nanotubes/butyl rubber composites prepared by a dry ice expansion pre-dispersion flocculation method. *J. Appl. Polym. Sci.* **139**(14), 51897 (2022)
26. B.-K. Zhu, S.-H. Xie, Z.-K. Xu, Y.-Y. Xu, Preparation and properties of the polyimide/multi-walled carbon nanotubes (MWNTs) nanocomposites. *Compos. Sci. Technol.* **66**(3), 548–554 (2006)
27. I.V. Gofman, K. Balik, M. Cerny, M. Zaloudkova, M.J. Goikman, V.E. Yudin, Peculiarities of the initial stages of carbonization processes in polyimide-based nanocomposite films containing carbon nanoparticles. *Cogent Chem.* **1**(1), 1076712 (2015)
28. Y. Wang, J. Sun, L.J.K.E.M. Dai, The properties of polyimide fibers modified by functionalized multi-wall carbon nanotubes based on friedel-crafts acylation. *Key Eng. Mater.* **727**, 490–496 (2017)
29. W. Chen, M. Ji, S.-Y. Yang, High thermal stable polyimide resins derived from phenylethynyl-encapped fluorenyl oligoimides with low melt viscosities. *Chin. J. Polym. Sci.* **34**(8), 933–948 (2016)
30. L. Jian, Effect of surface treatment on enhancing interfacial strength of carbon fiber/polyimide composites. *J. Thermoplast. Compos. Mater.* **35**(5), 708–719 (2020)
31. Y.-E. Miao, G.-N. Zhu, H. Hou, Y.-Y. Xia, T. Liu, Electrospun polyimide nanofiber-based nonwoven separators for lithium-ion batteries. *J. Power Sources* **226**, 82–86 (2013)
32. W. Yang, F. Liu, H. Chen, X. Dai, W. Liu, X. Qiu, X. Ji, Influence of heating rate on the structure and mechanical properties of aromatic BPDA-PDA polyimide Fiber. *Polymers* **12**(3), 510 (2020)
33. D. Lin, R. Li, T. Li, Y. Zi, S. Qi, D. Wu, Effects of pre-imidization on rheological behaviors of polyamic acid solution and thermal mechanical properties of polyimide film: an experiment and molecular dynamics simulation. *J. Mater. Sci.* **56**(26), 14518–14530 (2021)
34. R. Shokrani Havigh, H. Mahmoudi Chenari, A comprehensive study on the effect of carbonization temperature on the physical and chemical properties of carbon fibers. *Scientif. Rep.* **12**(1), 10704 (2022)
35. A. Thamizhlarasan, N. Murugan, Y.-C. Liu, R. Anbarasan, K.-L. Tung, Effect of amine and acid functionalization on polyimide: A structure-property relationship study. *React. Funct. Polym.* **173**, 105237 (2022)
36. D. Zhang, J. Dong, F. Gan, Z. Li, Q. Zhang, Structural evolution from poly(amic acid) to polyimide fibers during thermal imidization process. *High Perform. Polym.* **31**(5), 600–610 (2018)
37. D. Lin, M. Jiang, R. Li, S. Qi, D. Wu, Structure and properties of polyimide fiber prepared from polyamic acid solution with high solid content and low viscosity. *Mater. Lett.* **312**, 131628 (2022)
38. G.V. Vaganov, A.L. Didenko, E.M. Ivan'kova, A.G. Ivanov, I.L. Borisov, A.V. Volkov, Influence of temperature and imidization method on the structure and properties of polyimide fibers prepared by wet spinning. *Russ. Chem. Bull.* **71**(4), 760–765 (2022)
39. M. Kotera, T. Nishino, K. Nakamae, Imidization processes of aromatic polyimide by temperature modulated DSC. *Polymer* **41**(10), 3615–3619 (2000)
40. W. Chen, W. Chen, B. Zhang, S. Yang, C.-Y. Liu, Thermal imidization process of polyimide film: Interplay between solvent evaporation and imidization. *Polymer* **109**, 205–215 (2017)
41. I. Benfridja, S. Diahm, F. Laffir, G. Brennan, N. Liu, T. Kennedy, A universal study on the effect thermal imidization has on the physico-chemical, mechanical, thermal and electrical properties of polyimide for integrated electronics applications. *Polymers* **14**(9), 1713 (2022)
42. K.D.-H. Kim Beom-Kyung, C. Jae-Sun, K. Young-Ju, S. In-Seon, K. Soon-Ki, Molecular orientation of evaporated pentacene film on polyimide alignment layer. *Polymer (Korea)* **30**(4), 362–366 (2006)
43. W. Xu, Y. Ding, S. Jiang, J. Zhu, W. Ye, Y. Shen, H. Hou, Mechanical flexible PI/MWCNTs nanocomposites with high dielectric

- permittivity by electrospinning. *Eur. Polymer J.* **59**, 129–135 (2014)
44. M.A. Takassi, A. Zadehnazari, A. Farhadi, S. Mallakpour, Highly stable polyimide composite films based on 1,2,4-triazole ring reinforced with multi-walled carbon nanotubes: Study on thermal, mechanical, and morphological properties. *Prog. Org. Coat.* **80**, 142–149 (2015)
  45. H. Wei, L. Xu, J. Ren, L. Jia, Adsorption of bilirubin to magnetic multi-walled carbon nanotubes as a potential application in bound solute dialysis. *Colloids Surf., A* **405**, 38–44 (2012)
  46. M.-X. Tao, J.-S. Fan, J.-G. Nie, Seismic behavior of steel reinforced concrete column–steel truss beam hybrid joints. *Eng. Struct.* **56**, 1557–1569 (2013)
  47. D. An, T. Liu, H. Cui, Z. Chen, H. Xu, Y. Song, Study of the factors influencing load displacement curve of energy absorbing device by area division simulation. *Sci. Rep.* **12**(1), 13492 (2022)
  48. S.R. Goodyear, R.M. Aspden, Mechanical properties of bone ex vivo, in *Bone research protocols*. ed. by M.H. Helfrich, S.H. Ralston (Humana Press, Totowa, NJ, 2012), pp.555–571
  49. H. Sun, T. Wang, Y. Xu, W. Gao, P. Li, Q.J. Niu, Fabrication of polyimide and functionalized multi-walled carbon nanotubes mixed matrix membranes by in-situ polymerization for CO<sub>2</sub> separation. *Sep. Purif. Technol.* **177**, 327–336 (2017)
  50. S. Chen, L. Chen, Y. Wang, C. Wang, M. Miao, D. Zhang, Preparation of nanocomposites with epoxy resins and thiol-functionalized carbon nanotubes by thiol-ene click reaction. *Polym. Testing* **77**, 105912 (2019)
  51. A.C. Lua, J. Su, Effects of carbonisation on pore evolution and gas permeation properties of carbon membranes from Kapton polyimide. *Carbon* **44**(14), 2964–2972 (2006)
  52. M. Devi, S. Rawat, S. Sharma, A comprehensive review of the pyrolysis process: from carbon nanomaterial synthesis to waste treatment. *Oxford Open Mater. Sci.* **1**(1), itab014 (2021)
  53. B. Zhang, P. Wu, H. Zou, P. Liu, Morphology and properties of polyimide/multi-walled carbon nanotubes composite aerogels. *High Perform. Polym.* **30**(3), 292–302 (2017)
  54. W. Hao, X. Zhang, Tian thermal, mechanical, and microstructural study of PBO fiber during carbonization. *Materials* (2019). <https://doi.org/10.3390/ma12040608>
  55. P. Gutmann, J. Moosburger-Will, S. Kurt, Y. Xu, S. Horn, Carbonization of polyacrylonitrile-based fibers under defined tensile load: Influence on shrinkage behavior, microstructure, and mechanical properties. *Polym. Degrad. Stab.* **163**, 174–184 (2019)
  56. D.H.-D. Zhang Zhen-xing, L.I. Jia, G.A.N. Lin, C.H.I.A.N.G. Sum-wai, L.I. Bao-hua, K.A.N.G. Fei-yu, Preparation of aligned polyimide-based carbon nanofibers by electrospinning. *Newcarbon materials* **30**(4), 298–294 (2015)
  57. Z.-X. Zhang, H.-D. Du, J. Li, L. Gan, S.-W. Chiang, B.-H. Li, F.-Y. Kang, Preparation of aligned polyimide-based carbon nanofibers by electrospinning. *Carbon* **95**, 1082 (2015)
  58. K.S. Yang, D.D. Edie, D.Y. Lim, Y.M. Kim, Y.O. Choi, Preparation of carbon fiber web from electrostatic spinning of PMDA-ODA poly(amic acid) solution. *Carbon* **41**(11), 2039–2046 (2003)

Springer Nature or its licensor (e.g. a society or other partner) holds exclusive rights to this article under a publishing agreement with the author(s) or other rightsholder(s); author self-archiving of the accepted manuscript version of this article is solely governed by the terms of such publishing agreement and applicable law.